IEEE Access
Multidisciplinary | Rapid Review | Open Access Journal

Received January 3, 2019, accepted January 27, 2019, date of publication March 11, 2019, date of current version March 20, 2019.

Digital Object Identifier 10.1109/ACCESS.2019.2897793

Analyzing Ionosphere TEC and ROTI Responses on 2010 August High Speed Solar Winds

YANG LIU[1,2], (Member, IEEE), ZHENG LI[1], LIANJIE FU[1], JINLING WANG[3], SANDRO M. RADICELLA[2], AND CHUNXI ZHANG[1]

[1]School of Instrumentation and Opto-Electronic Engineering, Beihang University, Beijing 100191, China
[2]Abdus Salam International Centre for Theoretical Physics, Telecommunications/ICT for Development Laboratory, 34151 Trieste, Italy
[3]School of Civil and Environmental Engineering, University of New South Wales, Sydney, NSW 2052, Australia

Corresponding author: Yang Liu (liuyangee@buaa.edu.cn)

This work was supported in part by the National Key Research and Development Plan by Ministry of Science and Technology under Grant 2016YFC1402502, in part by the National Natural Science Foundation of China Innovation Group under Grant 61521091, in part by the National Natural Science Foundation of China under Grant 61771030 and Grant 61301087, in part by the 2011 Collaborative Innovation Center of Geospatial Technology, and in part by the China Scholarship Council.

ABSTRACT The high-speed solar winds stream (HSSWS) generated by coronal hole can produce large interplanetary magnetic field magnitude oscillations, leading to high latitude geomagnetic disturbances, and ionospheric responses as well. This paper has analyzed the global ionospheric total electron content (TEC) and rate of TEC index (ROTI) responses during the high speed solar winds stream occurred from 23 to 29 August, 2010. Ground Global Navigation Satellite System (GNSS) network was mainly used to investigate ionosphere TEC and ROTI behaviors. It has revealed that high latitudes and middle latitudes ionosphere suffered most during this event, with hemisphere asymmetry characteristics. Both TEC variations and ionosphere irregularities were analyzed. The HSSWS event brings to strong ionosphere irregularities represented by large ROTI enhancements at high latitudes. The concentrated ionosphere irregularities were closely related to the intensity of Auroral Electrojet enhancement activities. The ROTI enhancements at high latitudes, including polar cap, aurora, and sub-aurora are also influenced by solar zenith angle; all the prominent ROTI increments are observed in the ranges between 70° and 110° solar zenith angles; while the ROTI enhancements at low latitudes and equator are mostly found in the ranges between 130° and 170° solar zenith angles. The ionosphere disturbance triggered by the HSSWS is also noticed by some remarkable changes of F2 layer peak height. The work is contributing to the understanding of the theoretical coupling mechanism between high speed solar winds stream and magneto-ionosphere responses and provides a reference for space weather analysis and forecasting under similar events.

INDEX TERMS High speed solar winds stream, ionospheric TEC, ionosphere irregularity.

I. INTRODUCTION

The high speed solar winds stream generated by coronal hole can interact with low speed solar winds [1]; a typical HSSWS event can induce phenomena as: 1) elevated solar wind speed lasting for many days; 2) a pulse of elevated density forming a co-rotating interaction region (CIR); 3) enhanced magnetosphere convection persisting for days, producing magnetic IMF Bz oscillations; 4) enhanced wave-particle interactions in the inner magnetosphere; 5) enhanced particle precipitation in the aurora regions, with huge energy injected in combination of Joule heating procedure, followed by ionosphere TEC variations. Accompanied by electrodynamic perturbations, the effects of HSSWS then propagate down towards to middle and low latitude regions; followed by changes in thermosphere neutral wind circulation and enhanced magnetosphere convection, thus ionosphere in middle and low latitudes can be elevated, indicated by NmF2 and HmF2 changes observed by [2].

The ionosphere responses to HSSWS are manifested mainly by rapid TEC oscillations and generation of ionosphere irregularities. Considering the directionality characteristics of HSSWS, global responses usually show asymmetry features, as indicated by [3] and [4] studying a long lasting

The associate editor coordinating the review of this manuscript and approving it for publication was Mugen Peng.

HSSWS event. It was quite different from geomagnetic storms driven by coronal mass ejection (CME) where TEC variation induced by HSSWS was relatively weak and lasting a short period. The disturbance dynamo electric field (DDEF) induced by HSSWS can push ionosphere northwards or southwards, with reformation affecting the Equatorial Ionosphere anomaly (EIA). This anomaly is a feature of the non-uniform latitudinal distribution in ionospheric electron density, exhibiting two crests at magnetic latitudes around 15° north/south and a trough at the magnetic dip equator [5], [6]. It is mentioned also that the shape of EIA under HSSWS varied in correlation with the longitudes [7]. Presently most ionosphere TEC behaviors are is monitored by using ground based GNSS networks [8], such as the International GNSS Service (IGS); more topside ionosphere electron density changes are provided by in-situ instruments as supplements to further investigate reaction of topside ionosphere [9]. TEC variation in polar cap has been studied by ground GNSS observations provided from Canadian High Altitude Ionosphere Network (CHAIN); it shows that geomagnetic perturbations like sub-storms cause over 1 TECU variations, depending on seasons and local time; moreover, with multiple GNSS observables, the ionosphere disturbance propagation speed can be estimated. With TEC calculated from GNSS observations, particle precipitation can be well studied [10]–[12].

Particle precipitation further leads to expansion of polar gap, generating ionosphere irregularities and interfering trans-ionosphere propagation producing signal scintillation. It is assumed that most high latitudes scintillation phenomena are related to HSSWS events [13]. Other studies shows that both moderate and strong geomagnetic storms have consequences of ionosphere scintillation with varied intensities [14]–[16]. Ionosphere scintillation is measured by several scintillation index output from GNSS ionosphere scintillation monitor (ISM). However one of the most accepted metric for ionosphere irregularities and scintillations is ROTI proposed by [17], and this metric has been adopted in many related studies [18].

Longitudinal asymmetry and hemisphere asymmetry have been observed and discussed during the HSSWS induced ionosphere perturbations [19]. Most of these asymmetry or non-homogenous responses are attributed to the effect of solar illumination. It reveals that the impact of solar illumination is only regional in longitudes, depending on solar zenith angle; for the rest regions, the influence of heliospheric and geomagnetic drivers become dominant.

The HSSWS event from August 24th to August 28th 2010 was considered a typical case; the long durations of solar wind speed maintaining above 600km/s provides adequate information to study HSSWS effects on magnetic-ionosphere responses. It happened during solar minimum phase, when ionosphere properties under quiet condition were easily measured, setting up a good background for investigations of any disturbance. In this paper, the ionosphere effects of the HSSWS are mainly analyzed using IGS network data, with the addition of ionosondes data. The temporal and geophysical behaviors of TEC under HSSWS event from August 20th to August 30th were selected as a typical case study. The responses of ionosphere irregularities and scintillations were also investigated.

Section 2 describes data representation and proposed methodology. Section 3 presents analysis done to verify the response of ionosphere TEC enhancement, irregular ROTI behavior and cycle slips. The results are discussed in Section 4. Finally conclusions are given.

II. DATA PRESENTATION AND ANALYSIS FRAMEWORK

A. DATA PRESENTATION

The ionosphere response to HSSWS was analyzed by different sources of data, spanning from August 20th to August 30th 2010; with comparison, geomagnetic quiet days in August 2010 were also selected and considered (day of year (doy) 226, 231, 232, 233 and 234, 2010) according to the quiet days data from International Service of Geomagnetic Indices (ISGI: http://isgi.unistra.fr/). Data were divided by subclasses: (1) Data describing solar activities. Mainly solar wind speed measured by the Advanced Composition Explorer (ACE) in-situ satellite; the interplanetary southward magnetic value IMF Bz collected from OMNI data website (https://omniweb.gsfc.nasa.gov/). (2) Data describing the geomagnetic index. Kp, Dst, AE, AU, AL were collected from ISGI, and Kp indicates global daily geomagnetic variation, Dst indicates intensity of global geomagnetic disturbance; AU and AL show eastward and westward electro-jets in aurora region; AE is the difference between AU and AL (AE = AU-AL). (3) Ground GNSS data to calculate TEC and ROTI. Mainly IGS (ftp://garner.ucsd.edu/rinex/) data selected in America sector, European sector, Asian sector. The selected GNSS observatories from IGS with geographical coordinates are given in Figure 1. (4) Global ionospheric TEC grid products from IGS (ftp://gssc.esa.int/gnss/products/ionex/), to provide global picture of TEC and TEC variations. To further describe TEC behavior under HSSWS event, GNSS observatories considered are selected as northern American high latitude, European-African region and Asian-Australia region. (5) ionosonde data from Global Ionosphere Radio Observatory (GIRO), to provide foF2, hmF2 and bottom side TEC values. Two sites in American and European high latitudes are selected in this work.

B. CALCULATION OF TEC AND ROTI

Ground GNSS observations are used to derive TEC in the path between GNSS satellite and a given receiver. Each satellite has slant TEC according to its motion and coordinate related to the receiver, while considering ionosphere as a thin shell with fixed height, where TEC is concentrated, absolute vertical TEC can be produced to measure the status of ionosphere at a given pierce point. The raw TEC is calculated by geometry-free combination of dual-frequency GNSS

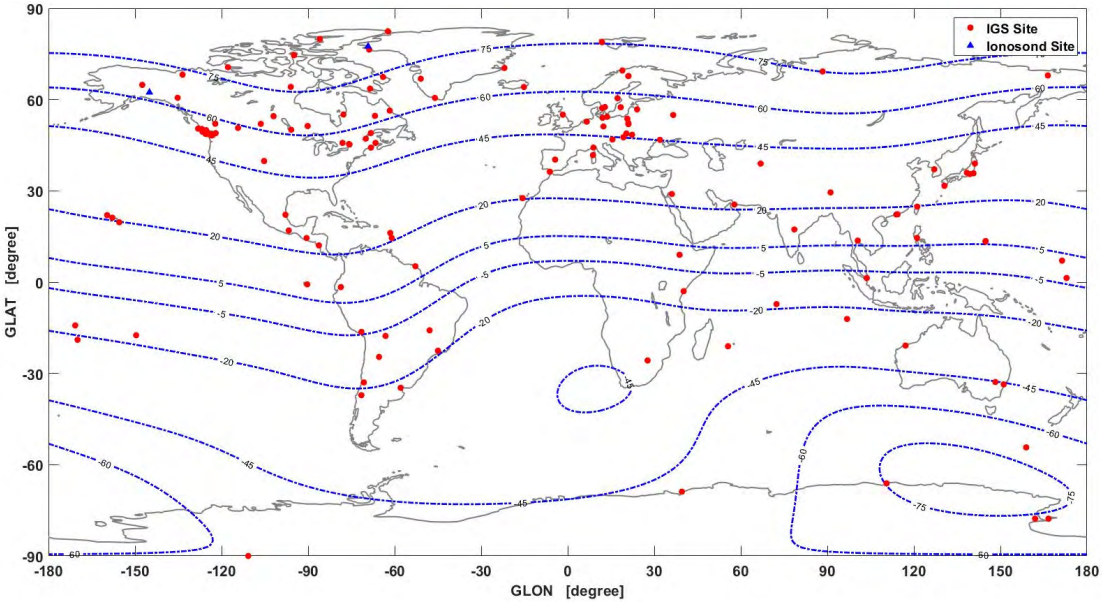

FIGURE 1. Stations for observation used for this work, the red dot indicates global IGS network, the blue triangle indicates selected ionosonde used in this work, the blue dashed line is geomagnetic dips; all the locations of station are presented in geographical coordinate.

observables, given by Eq.(1)

$$STEC = \frac{1}{40.3}\frac{f_1^2 f_2^2}{f_1^2 - f_2^2} \cdot \left[(\Phi_1 - \Phi_2) - (\lambda_1 N_1 - \lambda_2 N_2) + B_{r,s}\right] \tag{1}$$

where f_1 and f_2 are carrier frequencies of GPS dual frequencies signals; Φ_1 and Φ_2 are carrier phase measurements; λ_1 and λ_2 denote wave lengths of the dual-frequency GPS signals; N_1 and N_2 denote carrier ambiguities; $B_{r,s}$ is the bias between GPS satellites and receiver for carrier phase observations. Eq.(1) ignores the effects of carrier-phase multipath and noise. This raw TEC has carrier phase ambiguities and inter frequency bias; and the slant TEC is then estimated by Ciraolo's method [20], in the version used in the T/ICT4D Lab in International Centre for Theoretical Physics (ICTP). The TEC at ionosphere pierce point (IPP), defined as vertical TEC (VTEC), and is further derived by

$$VTEC = STEC \cdot \left[1 - \left(\frac{R_e \cos(\theta)}{R_e + H_{ipp}}\right)\right]^{-\frac{1}{2}} \tag{2}$$

where R_e represents averaging radius of the earth; θ is elevation angle in radians; H_{ipp} denotes average height of ionosphere pierce points, and considered 450km.

To further describe the disturbance of ionosphere TEC, linking with plasma variation, TEC rate of change index has been proposed by [17] and widely used by many researchers,. The rate of TEC is given as

$$ROT = \frac{STEC_{k+1} - STEC_k}{\Delta t_k} \tag{3}$$

where $STEC_{k+1}$ and $STEC_k$ are slat TEC at $k+1$ and k time epochs, respectively; Δt_k is time interval; usually the unit of ROT is TECU/min. When ROT is calculated during N epochs, ROTI is defined as

$$ROTI = \sqrt{\frac{1}{N}\sum_{j=1}^{N}\left(ROT_j - ROT_{aver}\right)^2} \tag{4}$$

where ROT_{aver} denotes averaging ROT during N epochs. A threshold of 0.5 TECU/min is considered as an indication of strong irregularities [17]. The relation between ROTI and scintillation indices has already been indicated in [21] to verify the assumption that ROTI is an indicator of ionosphere irregularity. $VTEC_{aver}$ is determined using the average TEC of five geomagnetic quiet days mentioned in sect. ***A.***

C. CALCULATION OF SOLAR WIND MAGNETOSPHERE COUPLING

The zonal component of motional solar wind electric field is defined as

$$E_y = V_{sw} B_z \tag{5}$$

where V_{sw} is solar wind speed in km/s unit, B_z is north-south component of the IMF in GSM coordinates, in nT unit. The reconnection electric field [22] is given as

$$E_R = V_{sw} B \sin^2\left(\theta/2\right) \tag{6}$$

B is Y-Z combined IMF in GSM coordinates, θ is calculated by arctan $\left(B_y/B_z\right)$.

Solar wind to magnetosphere coupling coefficient is described by Akasofu's function [23]:

$$\varepsilon = \frac{4\pi}{\mu_0} l_0^2 V_{sw} |B|^2 \sin^4\left(\theta/2\right) \tag{7}$$

$l_0 = 7R_e$ is a scaling factor, and R_e is the radium of earth

The solar wind kinetic energy flux [24] incident on one hemisphere of earth is defined by

$$W = \frac{1}{2}\left(\frac{1}{2}\rho V_{sw}^3\right)\left(\pi R_e^2\right) \tag{8}$$

III. EXPERIMENTS

A. GLOBAL MORPHOLOGY OF HSSWS INDUCED MAGNETOSPHERE-IONOSPHERE DISTURBANCE

The global morphology of this event is shown in Figure 2. The variables included and their behavior are:

1) IMF By (1 minute sampling), starting to drop below zero on 24th and then return back to positive values after several hours, with minimum value reaching to -20 nT;

2) IMF Bz (1 minute sampling), turned southward just few minutes after the burst of solar wind, and reaches peaked value around -10 nT at 6:50 UT. It oscillated during the whole phase of event, due to the rapid Alfven fluctuations;

3) The speed of solar wind (1 minute sampling), with component Vs, started to increase drastically at 03:50 UT 24th August, and reaching its maximum value of 728 m/s 5 hours later. It remained in a high level until 28th, and then decreased gradually to be less than 400 km/s;

4) The pressure of HSSWS (1 minute sampling), reached maximum value at 24th, after several hours of the burst of solar wind;

5) The reconnection electric field, calculated by Equation 6, shows similar pattern as By and Bz, reaching maximum value after the burst of solar wind, indicating the time that highest reconnection occurred;

6) Solar wind to magnetosphere coupling coefficient, calculated by Equation 7, started to drastically increase at 01:40 UT on 24th and reaching peak value after 1 hour;

7) Solar wind kinetic energy flux W, reached peak value at 01:40 UT on 24th, ahead of peak of the coefficient in the above panel of Figure 2(b);

8) Geomagnetic indices of Dst and Kp values, the Dst dropped to below –27.00 nT after the sudden commencement of the storm, and then gradually returned to normal values during the recovery phase of the HSSWS. The Kp kept relatively high values during the whole period of HSSWS, and then decreased; however the most Kp values were below 5.

9) AE,AU and AL values, the minimum AL value was −953 nT on 25th at 03:46 UT and the maximum AU value is 435 nT on 24th at 06:01 nT.

Obviously some energy had pulled into polar region and high latitudes, in case of the variations of AE, as discussed in [3]. The AE values have five periods of enhancements in following days; the first enhancement started at 10:00 UT 24th, and lasted for four hours; in this period, the solar wind coupled with magnetosphere, with highly energy transferring to ionosphere, and lead to a large reconnection electric field; the second enhancement began at 01:30 UT on 25th, and stopped at 05:30 UT for a short quiet period. Then followed the third enhancement, lasting from 07:30 UT to 13:30 UT in the same day; it should be noticed that this enhancement was the most severe among all AE responses. The fourth and fifth enhancements occurred on 27th, as the second phase of HSSWS, and finally ended at 12:30 UT on 27th.

B. GLOBAL TEC RESPONSES DERIVED FROM IGS IONEX DATA

To study the global TEC responses, IONEX data collected from IGS were analyzed during HSSWS period, as represented in Figure 3 (a and b), the vertical axis of first three subplots is geographical latitude (GLAT). Figure 3 (a) showed the global TEC variation for American sector, European-African sector and Asia-Australian sector respectively, at longitudes 70° W, 20° E and 130° E. It turns out that European-African sector suffers from the HSSWS event the most, keeping long time TEC enhancements in EIA, which is consistent with previous results [25], [26], indicating the main regions electro-jets affecting; the TEC in EIA was enhanced only on 24th and 25th in American sector, with clear hemisphere asymmetry observed, and northern part of EIA has dominant features. While in Asian-Australia sector TEC in EIA first gradually increased from 24th to 26th, and then decreased. The EIA has dominant features on 27th, during the second phase of HSSWS, corresponding to the four and fifth AE enhancements showed in Figure 2(b).

A critical feature is observed in Asian-Australian region on 27th, where the EIA decreased, compared with European-African sector. This can be explained by longitudinal influence on formation of ion density, indicating that thermosphere circulations and magnetic convections have comprehensive factors on ionosphere responses. Similar characteristics were observed in Figure 3(b), demonstrating variation of TEC differences.

Background TEC was calculated using the most geomagnetic quiet days' values, according to ISGI data. The increase of TEC was mainly discovered in equatorial and low latitudes, and kept for two days after HSSWS commencement in American sector, for four days in European-African sector. Certain TEC depletions were found after HSSWS in American high latitudes. Figure 3(c) discussed about EIA evolutions in the main phase of the HSSWS event, from 24th August to 27th August. An inhibition of EIA formation was observed in European sector, with the hump feature of TEC diminished by HSSWS force; the promotion of EIA formation started from 26th August in Asian-Australian sector, and becomes clear pattern one day later, with southern hemisphere a little bit dominant over the northern hemisphere in maximum TEC. In American region, the maximum TEC value appeared in northern hemisphere, in consistence with features revealed by Figure 3(a).

C. Local TEC RESPONSES

Local TEC responses at different geophysical locations are analyzed, the sites are selected in north and south hemispheres to represent TEC variations in polar cap, aurora, sub-aurora, middle latitudes, low latitudes and equatorial region,

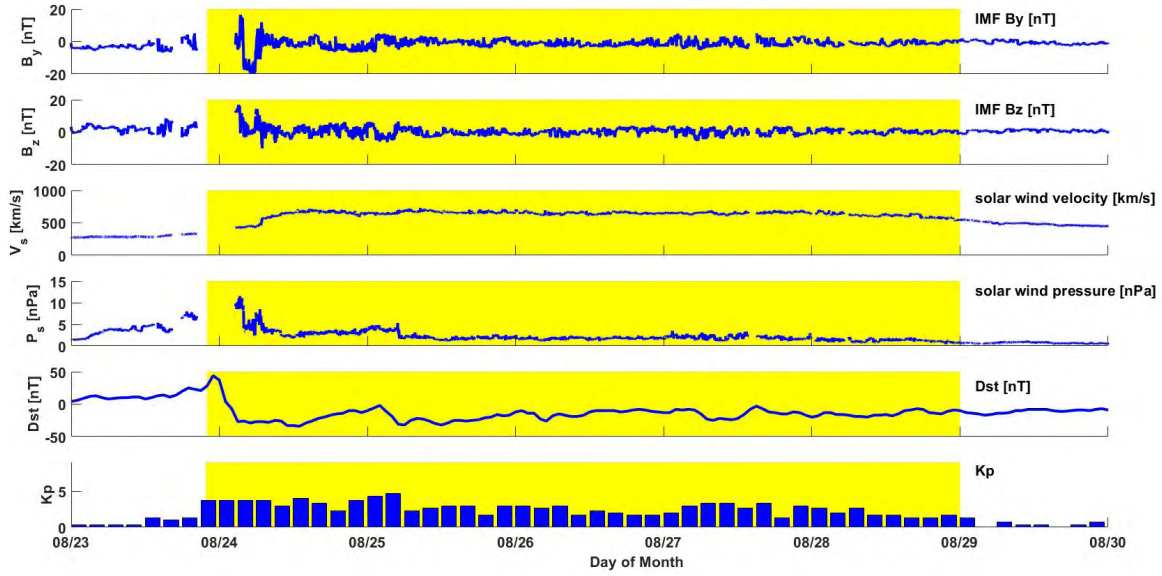

(a)

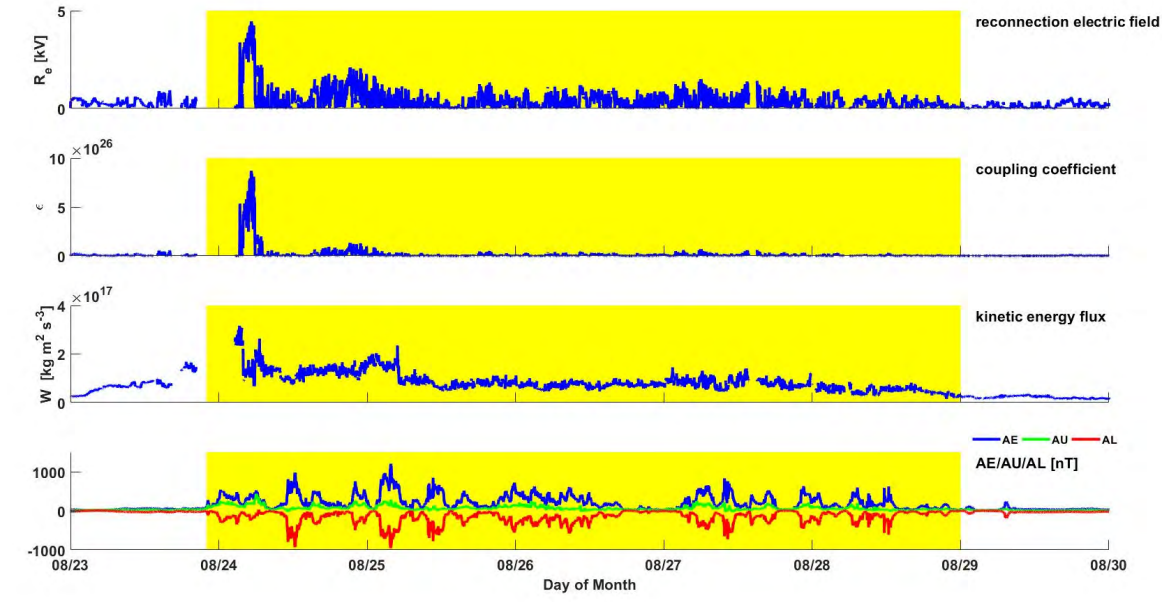

(b)

FIGURE 2. Global morphology of magnetosphere-ionosphere disturbance during the HSSWS, in (a) the IMF By and Bz, solar wind speed, the pressure and geomagnetic indices like Dst and Kp are demonstrated, in (b) the calculated reconnection electric field, coupling coefficient, energy flux and geomagnetic AE/AU/AL. the yellow paddings show the period of the HSSWS event.

as Figure 4 (a and b) shows. The blue lines denote averaged background VTEC derived from geomagnetic quiet days in the same month, the red lines denote VTEC variations under the HSSWS. To measure the VTEC disturbances, the standard deviations are calculated; VTEC variation percentage is used to distinguish the intensity of fluctuation in presence of the HSSWS. 1) **North hemisphere**: as it shows, it has fluctuations accompanied with slight depletion in north polar cap, as bake observatory found during the main phase of the HSSWS; but at the onset, VTEC was enhanced with fluctuations. VTEC was greatly enhanced during the first two days of the event in aurora region, as invk represented; then the slight depletion feature was noticed; similar features occurred in sub aurora, represented by clrs station,

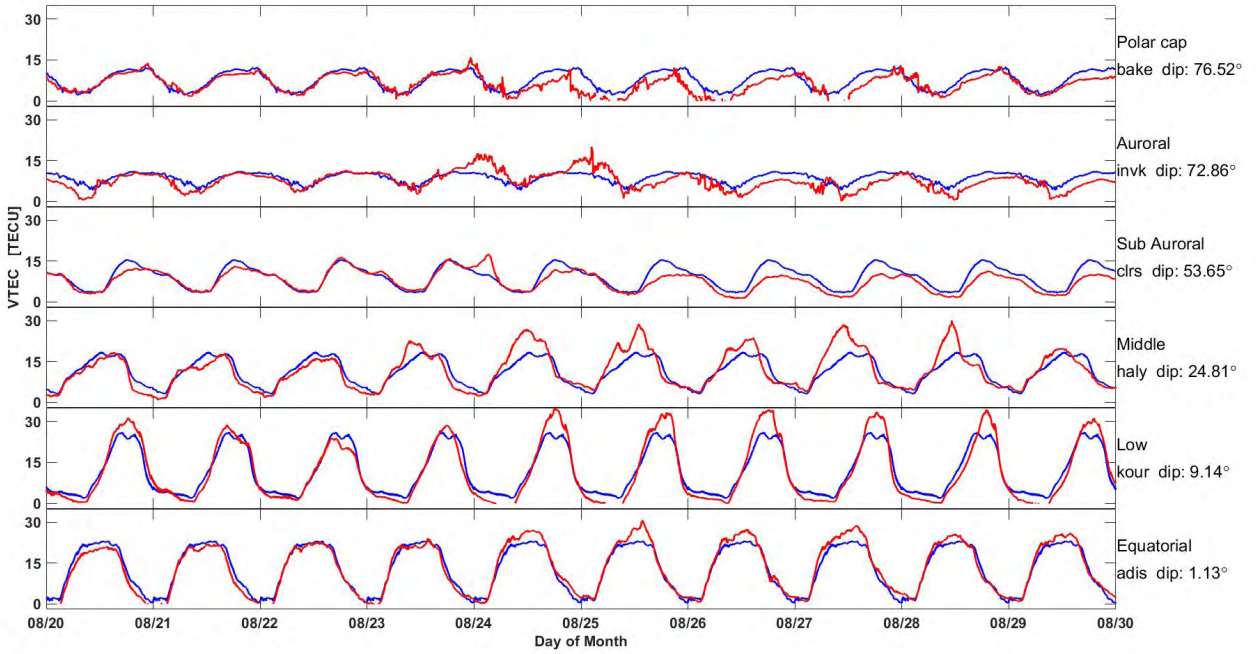

(a)

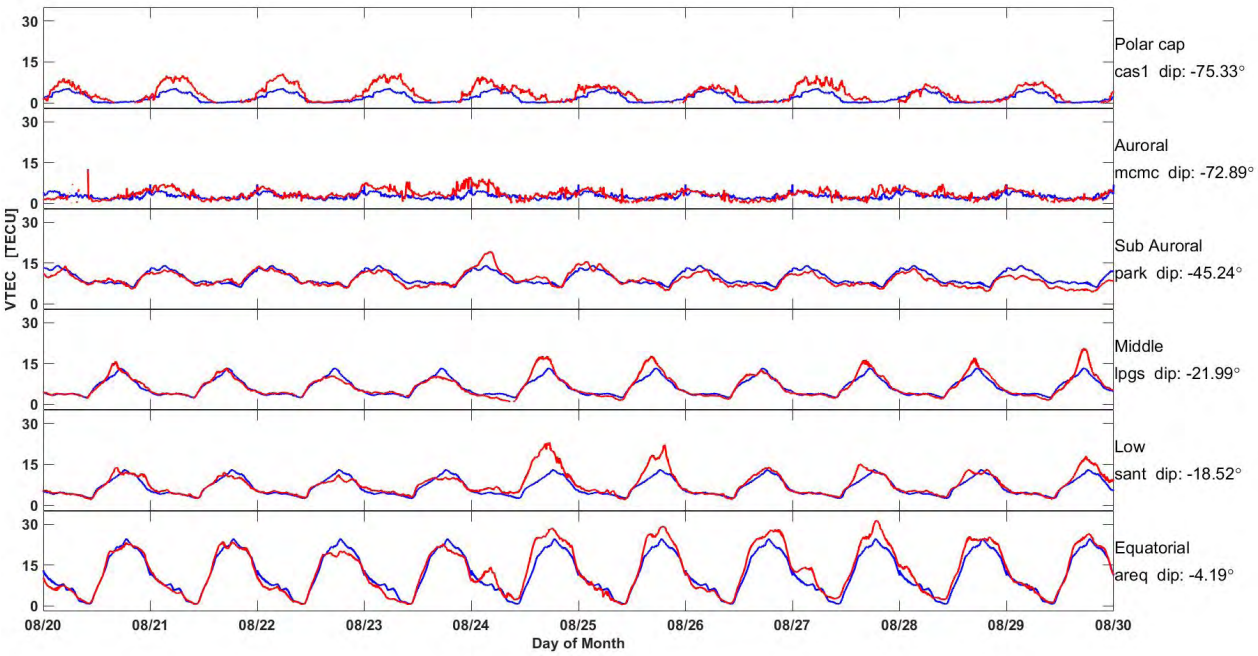

(b)

FIGURE 3. Local TEC responses to the HSSWS event (a) north Hemisphere and (b) south hemisphere, sites are selected from polar cap, aurora, sub-aurora, high latitude, middle latitude low latitude and equator.

remarkable increment during the first two days, the maximum VTEC variation exceed 77.35%. VTEC increment was found in middle latitudes during all phase of the event, as haly observatory discovered while in low latitudes, stations like kour, it shows that VTEC was increased in daytime and slightly decreased in night time, the most prominent enhancement happened at the noon sector; in the geomagnetic equator, the HSSWS also blooms the VTEC enhancement. 2) **South hemisphere**: in the south polar cap and south aurora, VTEC increased at the onset of storm, with 144.88% percentage; the VTEC increment was also observed at sub-aurora from 24^{th} to 26^{th}, and later the VTEC returned to its normal level;

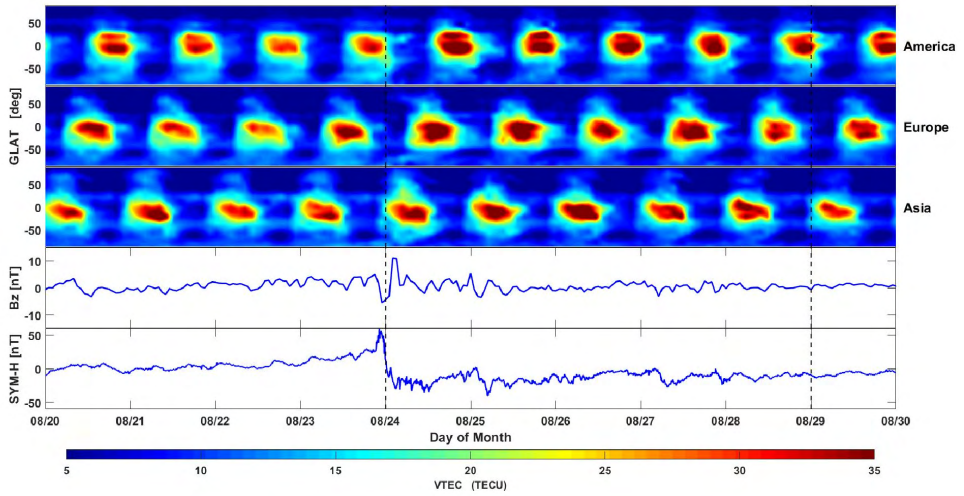

(a)

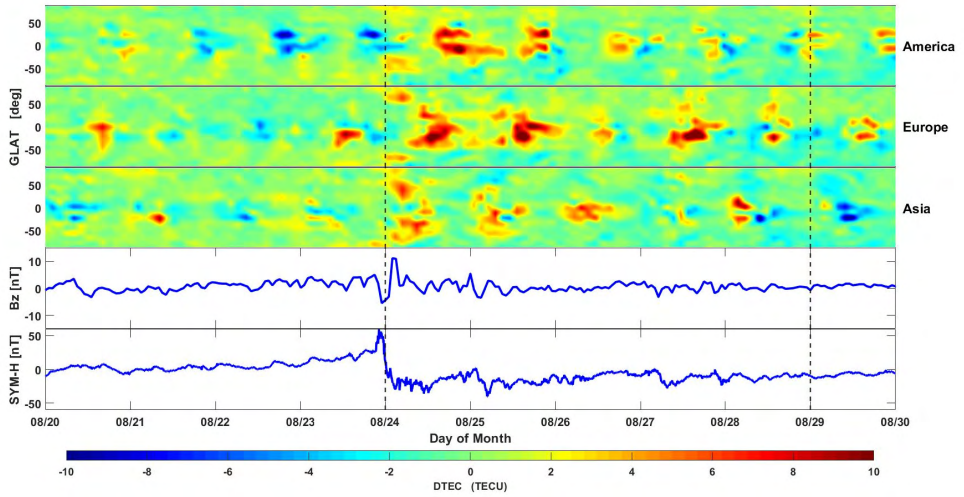

(b)

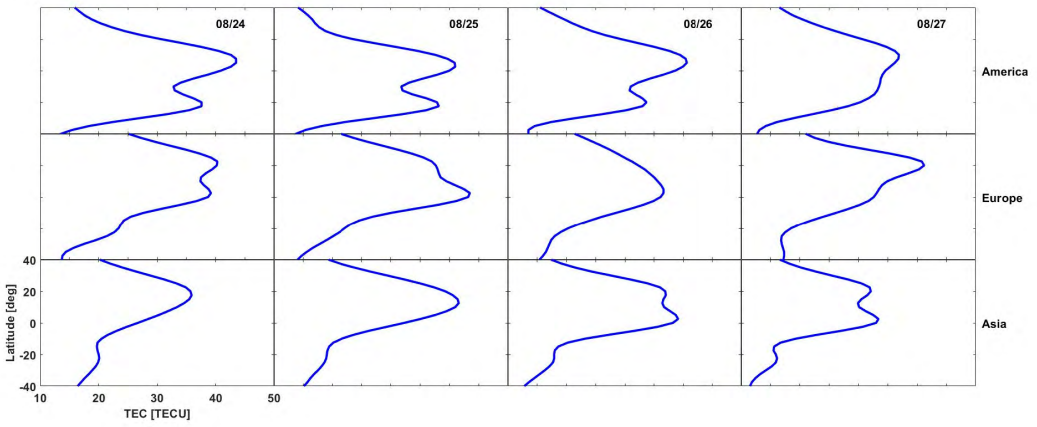

(c)

FIGURE 4. Global TEC responses to the HSSWS (a) TEC responses (b) TEC derivative responses (c) EIA, in (a) the color bar indicates VTEC values derived from global ionosphere map provided by IGS JPL data analysis center, (b) is also derived by the same data as (a), taking the average of geomagnetic quiet days as benchmark, the color bar indicates differential VTEC between HSSWS period and the benchmark; (c) is the EIA derived from global map, with fixed longitudes and fixed local time.

TABLE 1. Standard deviation of tec from selected stations.

region	Station	standard deviation (TECU)			variation percentage (%)
		background	HSSWS	HSSWS-background	
N polar cap	Bake	3.376	3.166	2.054	53.43
N auroral	Invk	1.892	3.248	2.457	72.73
N sub auroral	Clrs	3.974	3.617	2.097	77.35
N middle	Haly	5.091	6.819	3.470	50.15
N low	Kour	8.676	10.938	3.236	48.25
N equatorial	Adis	8.396	8.837	2.072	20.38
S equatorial	Areq	7.536	8.470	2.378	20.71
S low	Sant	3.137	4.076	2.052	94.63
S middle	Lpgs	3.165	3.987	1.561	68.26
S sub auroral	Park	2.325	2.596	1.388	49.76
S auroral	Mcmc	0.981	1.767	1.473	98.51
S polar cap	cas1	1.711	2.894	1.733	144.88

the VTEC increment in middle and low latitudes are less dominant than those in north hemisphere, denoted by lpgs and sant; a clear asymmetry pattern is present that VTEC is more influenced by the HSSWS during sunlit times, in sant station, VTEC value reached to over 94.63% percentage on 24th than its normal level in quiet condition, which is also dominant response for south hemisphere. A night side VTEC enhancement appeared just after the onset of the event, as areq station shows; during the HSSWS period, day time VTEC enhancements are the major response in areq station, however, the increment was not that strong as it discovered in north hemisphere. The VTEC standard deviation of these selected stations are calculated and shown in TABLE 1. The background TEC values are computed by averaging the geomagnetic quiet days (August 14th and August 22th). As it shows, north hemisphere suffers more TEC perturbations than south hemisphere, with increments of standard deviation values derived from the difference between the observed TEC under HSSWS and the background TEC. In aurora region, observed at invk, the increment of standard deviation is 2.457 TECU, while in middle latitudes represented by haly, the value is 3.470 TECU. Similar TEC standard deviation increments are found in low latitudes and equator of north hemisphere.

D. ROTI ENHANCEMENTS AT HIGH LATITUDES

To study the ionosphere irregularities during HSSWS, ROTI values were calculated in high latitudes of both two hemispheres. The ROTI enhancements to exceed a threshold of 0.2 TECU/min were considered a metric of ionosphere irregularities detection. As Figure 5 shows, observations from six sites are selected, three in north hemisphere and three in south hemisphere. In each hemisphere, the ROTI features under the HSSWS are studied, clear differences are found between polar cap and aurora. Most ROTI enhancements in polor cap and aurora are observed after the HSSWS commencement, with clear diurnal patterns. The different colors of plots indicate different measurements from satellites. Obvious hemisphere asymmetry response is noticed, with bake and invk in north hemisphere dominant. In north hemisphere, the response of ROTI can be divided into two stages, the first stage started from the onset time to the end of August 26th; the second stage lasted from August 27th to August 28th. While in south hemisphere, ROTI observed in mac1 in aurora region are active during the first two days of the event ROTI in mcm and cas1 keep almost same level, revealing less relevance with the HSSWS influence. For the diurnal patterns, in north hemisphere, most ROTI enhancements happened after sunset and ROTI intensity gradually decreased until midnight; a second enhancement happened after the midnight, which are prominent for bake, invk in north hemisphere. In south hemisphere, some daytime ROTI enhancements are noticed, but the strengths are relatively weak compared to the enhancements observed in north hemisphere. It shows that the HSSWS triggered ionosphere irregularities activities, therefore the ROTI values become more prominent. However, in general, ROTI values are larger during night time than day time in polar cap region. In aurora, the features of ROTI in response to the HSSWS varies on the locations. The high geomagnetic latitudes, the more severe ROTI intensity can be.

To further investigate relevance between AE, solar zenith angle and ROTI intensity. Twenty time spans are divided according to the AE activities, shown in Figure 6. In each time span, the starting and ending date and time are described in TABLE 2. ROTI intensity is statistically analyzed; results are shown in below. Figure 7(a) shows the ROTI intensity in respect with twenty time spans in American sector, obviously the polar cap and aurora regions are more sensitive to the AE enhancement. ROTI intensity increases with the onset of the HSSWS, and reached peak value at the sixth time span, when AE was also quite dominant; the fluctuation of ROTI intensity varies in accordance with AE perturbations. Another

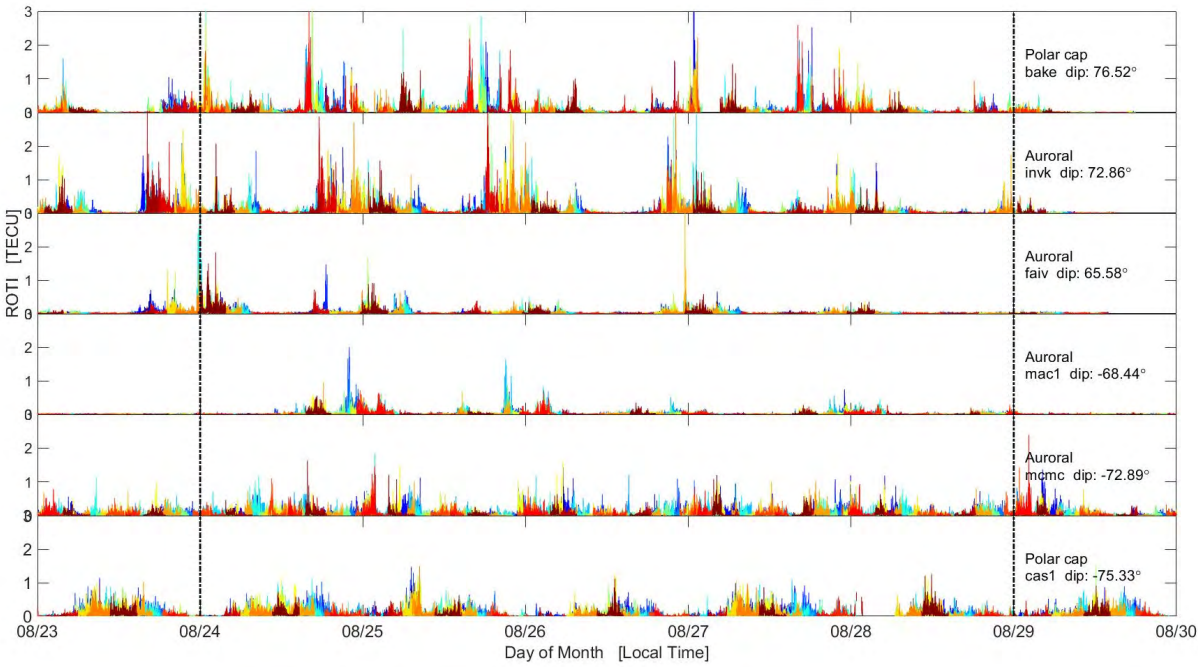

FIGURE 5. ROTI observed in Northern and Southern hemi-sphere, sites are selected from polar cap, aurora, sub-aurora, the different colors indicates different satellites; the two black dashed lines are the starting and ending time of the HSSWS event.

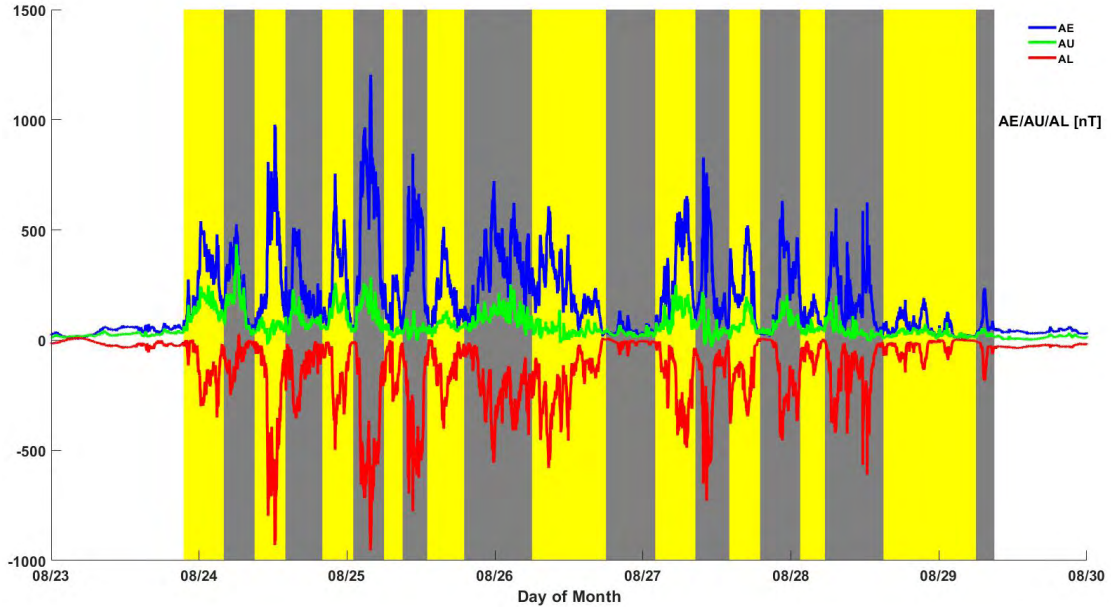

FIGURE 6. AE/AU/AL during the HSSWS events, each active period is highlighted; the red, blue and green lines show AE/AU/AL values.

prominent feature of ROTI intensity is found in low latitudes, compared with middle latitudes and equator. The high ROTI intensities are noticed during the first, second, sixth and seventh time spans. The two stage patterns of ROTI intensity can be observed in the features of low latitudes. Figure 7(b) represents the results of Asian sector, similar characteristics are discovered in polar and aurora regions, however the behaviors of low latitudes and equator are more remarkable compared with those of American sector, ROTI intensity is dominant in the eighth time span, when the maximum AE is 846 nT; a clear latency is noticed for the response of low latitudes and equator in Asian sector. Figure 7 (c) shows the results of European sector, the sub-aurora regions in Europe are prominent, the ROTI intensity increases just after the onset

TABLE 2. Details of each active period shown in figure 6, the number of each period is also linked with figure 7.

NO.	start day	Start UT	end day	end UT	MaxValue (nT)	Day(Max)	Time(Max)
1	23	21:30	24	04:00	540	24	00:17
2	24	04:00	24	09:00	526	24	06:02
3	24	09:00	24	14:00	978	24	12:17
4	24	14:00	24	20:00	510	24	15:18
5	24	20:00	25	01:00	756	24	22:04
6	25	01:00	25	06:00	1204	25	03:50
7	25	06:00	25	09:00	298	25	07:59
8	25	09:00	25	13:00	846	25	10:40
9	25	13:00	25	19:00	514	25	15:40
10	25	19:00	26	06:00	722	25	23:50
11	26	06:00	26	18:00	608	26	08:42
12	26	18:00	27	02:00	134	26	20:16
13	27	02:00	27	08:30	654	27	07:06
14	27	08:30	27	14:00	829	27	09:49
15	27	14:00	27	19:00	521	27	16:58
16	27	19:00	28	01:30	632	27	22:35
17	28	01:30	28	05:30	211	28	03:41
18	28	05:30	28	15:00	626	28	12:22
19	28	15:00	29	06:00	191	28	21:34
20	29	06:00	29	09:00	236	29	07:25

time, and then fluctuates with AE perturbations. The low latitudes and equator responses in Europe are noticeable in the twelfth time span, at the beginning of the second stage in the event. The longitudinal differences in response of the HSSWS are partially attributed to the sunlit effect, and also associated with local time. Since as time passed during the HSSWS period, ionosphere disturbance dynamo induced by the long time heating gradually becomes as major factor to control the ionosphere features in low latitudes and equator. During the daytime, DDEF has westward electric field, which inhibit formation of ionosphere irregularities in low latitudes and equator. However, after 21:30 LT at night, the change of direction facilitates the generation of irregularities, thus leads to increment of ROTI intensity.

Figure 8 shows the influences of solar zenith angle on ROTI responses during all the periods of HSSWS, the observations are taken from all IGS network data; clear longitudinal variations are observed from Figure 8 (a) to Figure 8 (c). It is indicated that sunlit has more influences on high latitudes, from polar cap to sub-aurora, where most prominent ROTI values occurred in the ranges of 70° to 100 ° of solar zenith angle. While the features of American equator in Figure 8(a) and European low latitudes in Figure 8(c) reveals dominant ROTI values in the ranges of 130° to 170° of solar zenith angle. The different behaviors are probably attributed to the mechanisms of ROTI enhancements. In high latitudes, from polar cap to sub-aurora, the generation of ROTI increments is particle precipitation and expansion of polar cap; the cause of ROTI increments at low latitudes and equators are mainly due to the pre-reversal enhancement, which speeds up the fountain effect, forming ionosphere irregularities.

E. ION DENSITY AND COMPOSITION VARIATIONS

Bottom side ionosphere responses were analyzed by ionosonde data provided by GIRO, two stations at high latitudes are selected study, one is GA762 and the other is THJ77. The data in GA762 is not quite continuous, compared with data of THJ77. In THJ77, a clear ionosphere height increment is discovered in F layer altitude, as Figure 9 demonstrates. A decrease of electron density started at the onset of storm, due to the temperature increase by continuous particle precipitations, and the consequent composition changes of F layer. It can be deduced that the height of ionosphere was lifted around 20km to 80km, depending on the thermosphere circulations, during the first stage of the HSSWS. It is noticed that the increase of F layer height was not directly corresponding to the AE enhancement, indicating the complex mechanism of HSSWS influence on ionosphere parameters. A possible explanation for this phenomenon is that the particle precipitation increase in high latitude during the HSSWS, leading to the increase of ionosphere temperature, followed by increase of the recombination rate. The more active of particle precipitation, the faster the recombination rate became. Then overall result is a decrease in density of ionosphere. Moreover, the increase in precipitation with

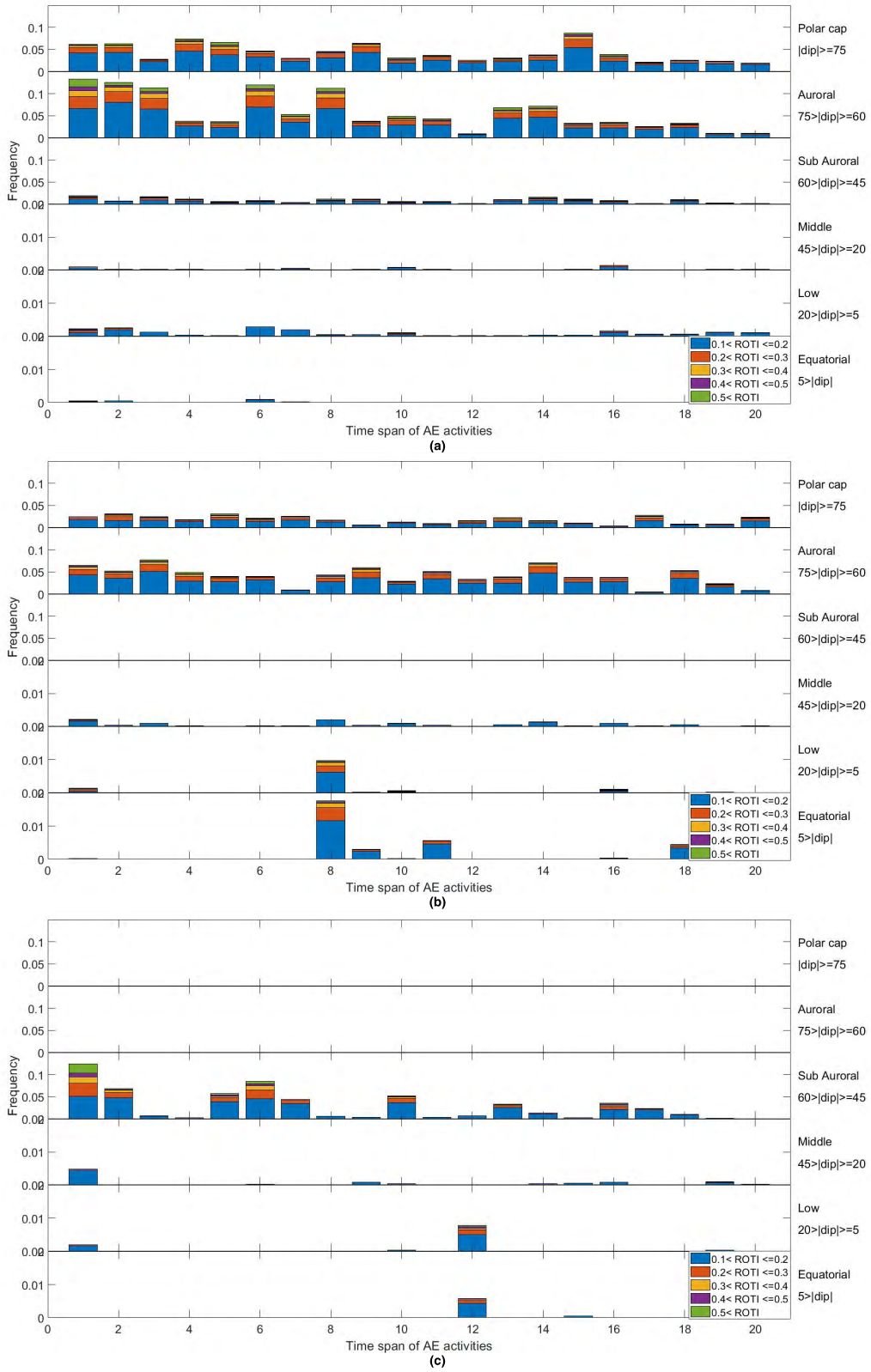

FIGURE 7. ROTI in response to each active AE period in northern hemisphere high latitudes, the color bar indicates ROTI intensity. (a) American sector. (b) Asian sector. (c) European sector.

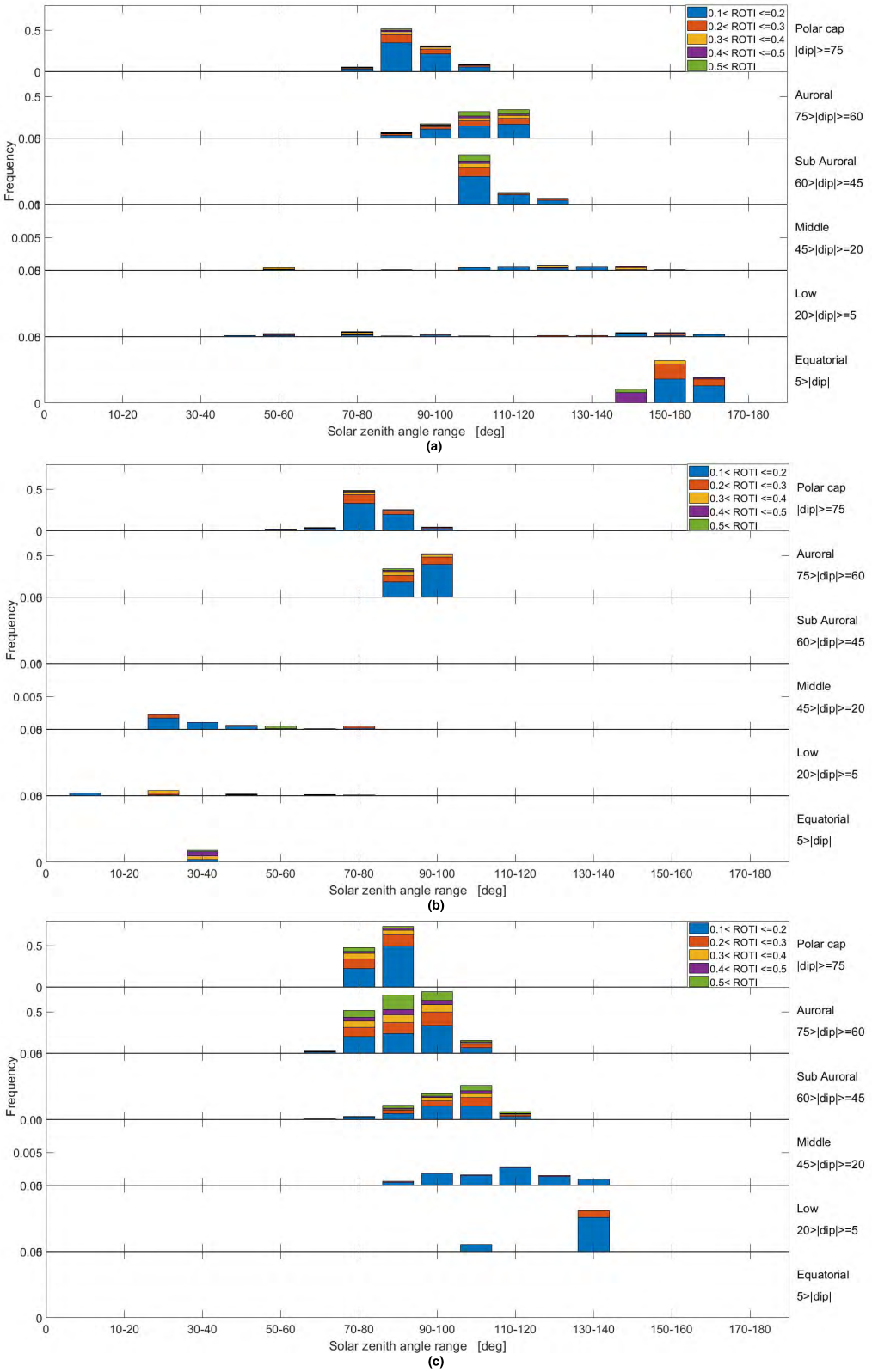

FIGURE 8. ROTI in response in relation with solar zenith angle, the solar zenith angles are binned with step of 10 degree. (a) American sector. (b) Asian sector. (c) European sector.

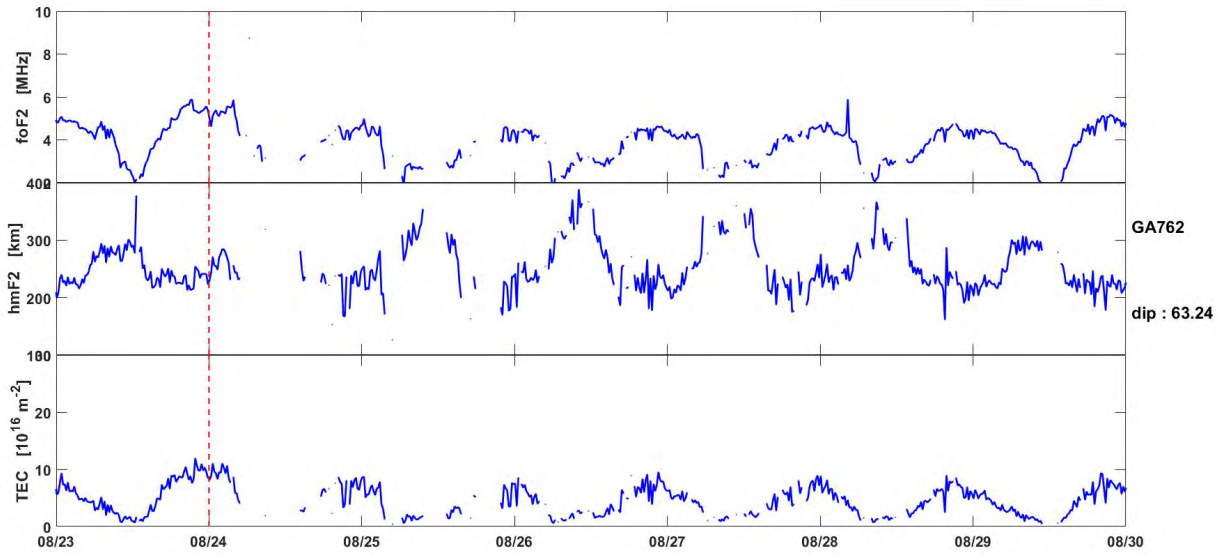

(a)

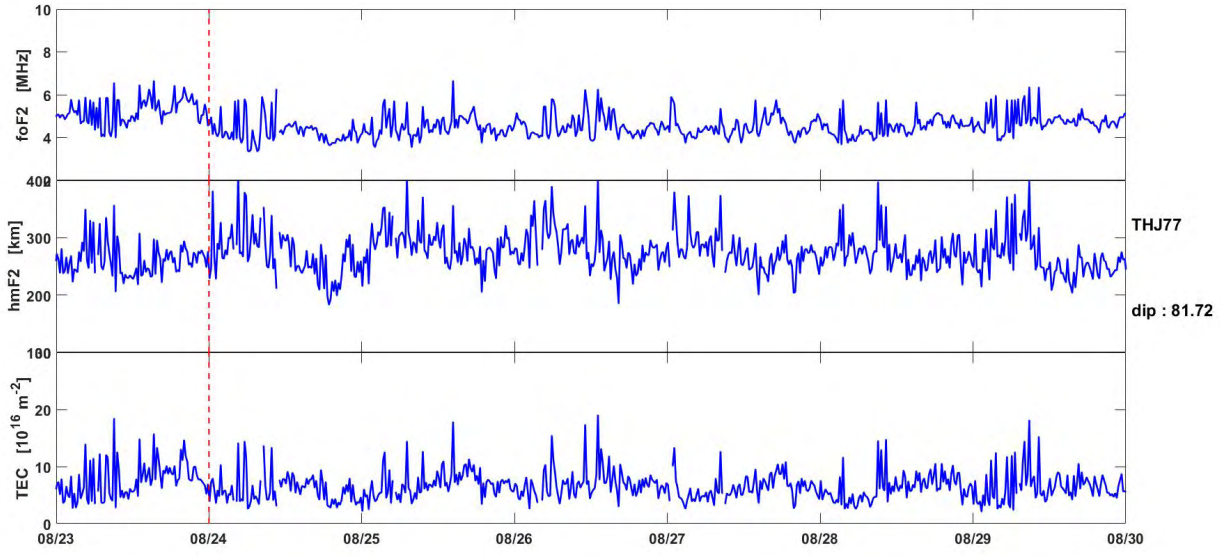

(b)

FIGURE 9. foF2, hmF2, and TEC derived from ionosonde at (a) GA762(62.38° N,145° W) and (b) THJ77 (77.5° N,69.2° W) during the HSSWS, the red dashed line shows the starting time of the HSSWS.

changes of thermosphere neutral wind circulation during magnetic convection also changed the height of ionosphere. The peak height of F layer ionosphere was strongly uplifted from August 25th to August 26^{h}; the variation of peak height also followed a diurnal pattern, while the drops of peak height happened after 00:30 UT. In GA762, the bottom side TEC is first enhanced after the onset of the event, then during the rest of the HSSWS period, the bottom side TEC has several perturbations, but with less magnitude than those at the beginning of the HSSWS. The peak height of F layer has a steeper increment rate, compared to THJ77. This is because THJ77 is located in polar cap and GA762 is located in sub-aurora, the diurnal pattern in GA762 is more prominent, since the variation of ionosphere is influenced by solar illuminations.

IV. DISCUSSION

A. IONOSPHERE TEC RESPONSES

The observations of TEC reveal noticeable varying responses in ionosphere to this HSSWS event. The varying features demonstrated in Figure 3 and Figure 4 were attributed to

TABLE 3. Standard deviation of tec from selected stations (2010-08-01 to 2010-08-09).

Region	Name	Back(TECU)	CME(TECU)	CME-Back(TECU)
Polar cap	bake	3.376	3.031	2.075
Auroral	dubo	3.728	3.880	1.964
Sub Auroral	amu2	4.004	7.552	8.331
Middle	mana	10.583	9.374	3.853
Low	hyde	10.497	10.688	3.986
Equatorial	adis	8.396	8.609	2.962

both latitudinal and longitudinal dependences. The TEC responses varied greatly in latitudinal locations; by dividing the observatories into polar cap, aurora, sub-aurora, middle latitudes, low latitudes and equator, it is obvious to see the asymmetry between north hemisphere and south hemisphere. At the beginning of this event, particles precipitation at high latitudes heated up the ionosphere, resulting in TEC enhancements in polar cap, aurora and sub-aurora; while the responses of TEC has some latency for low latitudes and equator, since in these regions TEC responses are more affected by DDEF, which has westward electric field at day time, prohibiting the formation of equatorial plasma bubbles. Another factor is supposed to attribute to the neutral wind, the equator-ward neutral wind during the HSSWS helped increase the electron density of upper latitudes, which is responsible at the beginning of the event.

TEC enhancements were found in middle latitudes, both northern and southern hemispheres just after the HSSWS commencement at European and American sectors. But in some Asian locations, TEC enhancements were delayed, indicating the direction and phase of ionospheric dynamo strength [27], [28]. The bottom TEC decrement observed in THJ77, with related raising of F2 peak heights, are in consistence with related studies [2].

The ionosonde results in Figure 8 also indicated some negative TEC decrease responses occurred at high latitudes, the explanations of this phenomenon were complex: could be related to composition changes, penetration of electronic field and thermosphere winds could contribute to the change of TEC. A global hemisphere asymmetry is discovered, which can be explained due to the positive IMF Bz and negative IMF By conditions, to enhance HSSWS response in northern hemisphere [3], [4]. The seasonal variation plays important role on the north-south asymmetry. Since the storm occurred in August, when the Northern hemisphere is better illuminated than the Southern one, thus the ionization in northern hemisphere is more active than in southern hemisphere. More solar illuminations are received at northern hemisphere, as Figure 8 revealed, the hemisphere asymmetry is in accordance with the effect of solar zenith angle. The TEC variations mainly concentrated after HSSWS commencement, when the reconnection electric field and HSSWS magnetosphere coupling coefficient reached maximum values [29], [30]. During the event, the magnetosphere convection electric field increased the prompt penetration electric field (PPEF), as equation (5) represented.

The EIA changes showed in Figure 3 indicated that near equatorial region DDEF also played important role during this event. The results indicated penetration of magnetosphere electric field into middle and low latitudes, controlled by the IMF Bz, and had influences on ionosphere, as [2] previously discussed, addressing that CIR/HSSWS can raise the height of F layer ionosphere; while other studies consider that the fluctuations of IMF Bz can induce a significant increase of electron density [31], but not in the case for this event, as shown by the results of THJ77 ionosonde, the increments or depletion of TEC are also related with local time, for which the direction of PPEF changes between day and night.

The TEC perturbations by the HSSWS are compared with features during a geomagnetic storm at the same month (August 4^{th} to August 8^{th}), which was considered to driven by CME. It shows that the absolute VTEC values were greatly enhanced in middle latitudes, with dominant standard deviation up to 11.148 TECU, compared to the 10.688 TECU under CME-driven geomagnetic storm. The features of sub-aurora region were prominent for the both two events, with standard deviation over 7 TECU. For the rest regions, it seemed that CME-driven storm has more severe impacts on TEC perturbations than the HSSWS, but the gap is not large.

B. INHIBITIONS OF EIA FORMATIONS

At low latitudes, a noticeable HSSWS influence on EIA formation was found. [10] states that the high speed streams can play a significant role on EIA, with combined mechanisms by PPEF, DDEF and AE perturbations, leading to low latitudes ionosphere hmF2 and foF2 perturbations. As [32] and [33] stated PPEF is regulated by magnetic convections and acts as main force of vertical drift of ions, producing fountain effects in low latitudes F layer ionosphere. In this event, effects of DDEF, related to the disturbance of neutral winds generated and controlled by dynamo effect, were also dominant, driven by thermosphere winds, as sub-consequence of particle precipitations and Joule heating. Longitudinal asymmetry was demonstrated in EIA responses of the HSSWS, day time EIA formation was strongly inhibited in European region with development of HSSWS, while in Asian region day time EIA was first inhibited and then gradually turn promotion. The inhibition of EIA in American region was lighter, but

TABLE 4. Standard deviation of tec from selected stations (2010-08-20 to 2010-08-29).

Region	Name	Back(TECU)	HSSWS(TECU)	HSSWS-Back(TECU)
Polar cap	bake	3.376	3.165	2.058
Auroral	dubo	3.728	3.587	1.378
Sub Auroral	amu2	4.004	6.410	7.249
Middle	mana	10.583	11.148	3.884
Low	hyde	10.497	11.248	3.235
Equatorial	adis	8.396	8.862	2.043

was completely on 27th, during the second main phase of HSSWS, in accordance with AE perturbations. The increase of N2 density help to speed up loss of ionization and a decrease of O density reduce ionization production, thus the decrease of O/N2 indicated decrease of electron density in F layer ionosphere. This HSSWS brought up global increments of O/N2 and electron density after 25th, while the inhibition of EIA continued to grow, which lead to disagreements with previous results indicated by [34]. The composition changes are assumed to be formed in the auroral region by Joule heating and then propagated downward to middle and low latitudes by combined force of background wind and HSSWS-concentrated wind. A probable explanation for that is the effects of neutral winds during the HSSWS, as [35] addressed, the neutral winds and composition effects result in an asymmetric response of EIA. Another supplement explanation for inhibition of EIA is the electric field effect during HSSWS, as [30] and [33] proved that electric field could be a major driver in producing simultaneous EIA variations during magnetic perturbations.

C. IONOSPHERE IRREGULARITIES AND ROTI ENHANCEMENTS

A large scale of irregularities has been produced by the HSSWS event at high latitudes. The dominant ROTI observations indicate ionosphere scintillations occurred during the HSSWS. Large ROTI values were discovered in European, Canadian and Russian high latitudes, with different intensities. The results in Figure 5 were in accordance with observations reported by [14] and [15], through investigation of CHAIN data. The signatures of ionosphere irregularities observed in this HSSWS event were different from those reflections occurred at low latitudes and equatorials during geomagnetic storms, which highly depended on event commencement local time, the strengths and directions of zonal electro-magnetic fields [36]–[38], as Figure 7 demonstrates. The concentration of ionosphere irregularities was closely related to intensity of AE perturbations, indicating the major cause of high latitudes ionosphere irregularities. While the irregularities generated in low latitudes and equators are attributed to eastward electric field at night side, accelerating the Rayleigh-Taylor instability and push up the F region ionosphere.

In the auroral zone, the precipitation increased the conductivities and generated Joule heating. The Joule heating heats the neutral atmosphere and increased the temperature, changing the rate of collision and finally change the composition [30]. The Joule heating also produced a motion of thermosphere winds which generated a disturbance of ionosphere dynamo and as a consequence disturbance of geomagnetic field on the daysides [29].

The ROTI responses behaved strong hemisphere asymmetry feature, as also proved by [3] and [4]. The results were in consistence with previous conjugating asymmetry studies of the similar events [39], in which scintillations between northern and southern high latitudes were carefully compared. Even at the same level, ROTI responses vary from polar cap, aurora, sub-aurora and middle altitudes, from the analysis of America, Europe and Asia sectors, polar cap and aurora of America and Europe are more influenced than Asia; for all the three sectors, ROTI activities in middle latitudes are the weakest.

V. CONCLUSIONS

In this work, ionosphere responses to August 2010 HSSWS event were discussed. Our investigations have revealed some features as follows:

1) This event has significant effects on high latitude magneto-ionosphere system, which lasted about five days. The magnetic disturbances were in consistent with input energy strength by the HSSWS through magneto-sphere to ionosphere. HSSWS magneto-sphere coupling coefficient reached maximum when IMF By and Bz dropped down.
2) Global TEC variations were generated by penetration electric field and disturbance electric field together in ionosphere, with differences depending on latitudinal and longitudinal characteristics. About 144.88% TEC increment was observed at south hemisphere aurora region after the onset of HSSWS, while the averaging TEC enhancement in north hemisphere was over 50%. The above percentages are calculated from selected stations. In general, TEC perturbations were more dominant in north hemisphere than south hemisphere, during the full phase of the HSSWS. The standard deviations of TEC from selected stations show that north hemisphere suffered more about the TEC perturbations, with north middle latitudes dominant, the standard deviation value exceeds 3 TECU. In longitudinal view, European and African sector have the most severe response than Asia.

3) The HSSWS event brings to strong ionosphere irregularities represented by large ROTI enhancements at high latitudes. The concentrated ionosphere irregularities were closely related with intensity of AE enhancement activities. The cause of such ROTI enhancements in America and Europe sectors is also attributed to long lasting Joule heating during the HSSWS, the increasing temperature in ionosphere changes recombination coefficient, and speeds up the formation of ionosphere irregularities in polar cap and aurora region. Some prominent ROTI increments are found in low latitudes and equator of Europe and Asia sector; the enhanced eastward electric field is responsible for these features, by strengthen the force of $\mathbf{E}\times\mathbf{B}$, accelerating the formation of equatorial plasma bubbles. The ROTI enhancements at high latitudes, including polar cap, aurora and sub-aurora are also influenced by solar zenith angle; all the prominent ROTI increments are observed in the ranges between 70° and 110° solar zenith angles; while the ROTI enhancements at low latitudes and equator are mostly found in the ranges between 130° and 170° solar zenith angles.
4) The ionosphere disturbance triggered by the HSSWS is also noticed by some remarkable changes of F2 layer peak height. Despite the diurnal variations of F2 layer peak height, perturbations are observed at high latitudes observatories. Bottom side TEC increments occurred at the same locations, just after the onset of the HSSWS.
5) The global responses of this HSSWS event have hemisphere asymmetry features. Northern hemisphere reacts more sensitive than southern hemisphere conjugating points. Responses at similar geomagnetic latitude vary due to longitudinal dependence. America and Europe sectors have more sensitive responses than Asia, partially due to the sunlit effects at the HSSWS commencement, when these two sectors had less solar illumination than Asia sector. Further investigations are needed to discuss the hided complex mechanism.

ACKNOWLEDGMENT

The authors would like to thank the reviewers for their detailed and insightful comments and constructive suggestions. Special thanks to all providers of data used (OMNIweb from NASA Goddard Space Flight Center to provide IMF Bz, solar wind data; International Services of Geomagnetic Indices to provide Dst and Kp data, International GNSS Service to provide GPS data, Global Ionosphere Radio Observatory to provide ionosonde data) in this research.

REFERENCES

[1] J. G. Lyon, "The solar wind-magnetosphere-ionosphere system," *Science*, vol. 288, no. 5473, pp. 1987–1991, 2000.
[2] M. H. Denton, T. Ulich, and E. Turunen, "Modification of midlatitude ionospheric parameters in the F2 layer by persistent high-speed solar wind streams," *Space Weather*, vol. 7, no. 4, pp. 1–10, Apr. 2009.
[3] N. Zaourar, C. Amory-Mazaudier, and R. Fleury, "Hemispheric asymmetries in the ionosphere response observed during the high-speed solar wind streams of the 24–28 August 2010," *Adv. Space Res.*, vol. 59, no. 9, pp. 2229–2247, 2017.
[4] A. J. de Abreu *et al.*, "Hemispheric asymmetries in the ionospheric response observed in the American sector during an intense geomagnetic storm," *J. Geophys. Res., Space Phys.*, vol. 115, no. A12, 2010, Art. no. A12312.
[5] E. V. Appleton, "Two anomalies in the ionosphere," *Nature*, vol. 157, p. 691, May 1946.
[6] K. F. Li *et al.*, "The 11 year solar cycle response of the equatorial ionization anomaly observed by GPS radio occultation," *J. Geophys. Res., Space Phys.*, vol. 123, no. 1, pp. 848–861, 2018.
[7] R. M. Skoug *et al.*, "Extremely high speed solar wind: 29–30 October 2003," *J. Geophys. Res., Space Phys.*, vol. 109, no. A9, pp. A09102.1–A09102.9, 2004.
[8] R. Tiwari, H. J. Strangeways, S. Tiwari, and A. Ahmed, "Investigation of ionospheric irregularities and scintillation using TEC at high latitude," *Adv. Space Res.*, vol. 52, no. 6, pp. 1111–1124, 2013.
[9] C. Xiong, H. Lühr, and B. G. Fejer, "The response of equatorial electrojet, vertical plasma drift, and thermospheric zonal wind to enhanced solar wind input," *J. Geophys. Res., Space Phys.*, vol. 121, no. 6, pp. 5653–5663, 2016.
[10] C. Watson, P. T. Jayachandran, and J. W. MacDougall, "Characteristics of GPS TEC variations in the polar cap ionosphere," *J. Geophys. Res., Space Phys.*, vol. 121, no. 5, pp. 4748–4768, 2016.
[11] C. Watson, P. T. Jayachandran, and J. W. MacDougall, "GPS TEC variations in the polar cap ionosphere: Solar wind and IMF dependence," *J. Geophys. Res., Space Phys.*, vol. 121, pp. 9030–9050, Sep. 2016.
[12] C. Watson, P. T. Jayachandran, E. Spanswick, E. F. Donovan, and D. W. Danskin, "GPS TEC technique for observation of the evolution of substorm particle precipitation," *J. Geophys. Res., Space Phys.*, vol. 116, no. A10, pp. 1–15, 2011.
[13] J. Liu, L. Liu, B. Zhao, Y. Wei, L. Hu, and B. Xiong, "High-speed stream impacts on the equatorial ionization anomaly region during the deep solar minimum year 2008," *J. Geophys. Res., Space Phys.*, vol. 117, no. A10, 2012, Art. no. A10304.
[14] P. Prikryl *et al.*, "GPS phase scintillation and proxy index at high latitudes during a moderate geomagnetic storm," *Annales Geophysicae*, vol. 31, no. 5, pp. 805–816, 2013.
[15] P. Prikryl *et al.*, "GPS phase scintillation at high latitudes during geomagnetic storms of 7–17 March 2012–Part: The North American sector," *Annales Geophysicae*, vol. 33, no. 6, p. 637. 2015.
[16] I. Cherniak and I. Zakharenkova, "New advantages of the combined GPS and GLONASS observations for high-latitude ionospheric irregularities monitoring: Case study of June 2015 geomagnetic storm," *Earth, Planets Space*, vol. 69, no. 1, p. 66, 2017.
[17] X. Pi, A. J. Mannucci, U. J. Lindqwister, and C. M. Ho, "Monitoring of global ionospheric irregularities using the worldwide GPS network," *Geophys. Res. Lett.*, vol. 24, no. 18, pp. 2283–2286, 1997.
[18] I. Cherniak, I. Zakharenkova, and A. Krankowski, "The approaches for ionosphere irregularities modeling on base of ROTI mapping," *Earth Planets Space*, vol. 66, no. 1, p. 165, 2014.
[19] A. V. Dmitriev, C.-M. Huang, P. S. Brahmanandam, L. C. Chang, K.-T. Chen, and L.-C. Tsai, "Longitudinal variations of positive dayside ionospheric storms related to recurrent geomagnetic storms," *J. Geophys. Res., Space Phys.*, vol. 118, no. 10, pp. 6806–6822, 2013.
[20] L. Ciraolo, F. Azpilicueta, C. Brunini, A. Meza, and S. M. Radicella, "Calibration errors on experimental slant total electron content (TEC) determined with GPS," *J. Geodesy*, vol. 81, no. 2, pp. 111–120, 2006.
[21] Z. Yang and Z. Liu, "Correlation between ROTI and Ionospheric Scintillation Indices using Hong Kong low-latitude GPS data," *GPS Solutions*, vol. 20, no. 4, pp. 815–824, 2016.
[22] J. R. Kan and L. C. Lee, "Energy coupling function and solar wind-magnetosphere dynamo," *Geophys. Res. Lett.*, vol. 6, no. 7, pp. 577–580, 1979.
[23] S.-I. Akasofu, "Energy coupling between the solar wind and the magnetosphere," *Space Sci. Rev.*, vol. 28, no. 2, pp. 121–190, 1981.
[24] A. Olsson, P. Janhunen, T. Karlsson, N. Ivchenko, and L. G. Blomberg, "Statistics of Joule heating in the auroral zone and polar cap using Astrid-2 satellite Poynting flux," *Annales Geophysicae*, vol. 22, no. 12, pp. 4133–4142, 2004.

[25] B. G. Fejer and L. Scherliess, "Time dependent response of equatorial ionospheric electric fields to magnetospheric disturbances," *Geophys. Res. Lett.*, vol. 22, no. 7, pp. 851–854, 1995.
[26] C. H. Lin *et al.*, "Theoretical study of the low- and midlatitude ionospheric electron density enhancement during the October 2003 superstorm: Relative importance of the neutral wind and the electric field," *J. Geophys. Res. Space Phys.*, vol. 110, NO. A12, 2005.
[27] A. Shimeis *et al.*, "TEC variations along an East Euro-African chain during 5th April 2010 geomagnetic storm," *Adv. Space Res.*, vol. 55, no. 9, pp. 2239–2247, 2015.
[28] R. Singh *et al.*, "Low-latitude ionosphere response to super geomagnetic storm of 17/18 March 2015: Results from a chain of ground-based observations over Indian sector," *J. Geophys. Res., Space Phys.*, vol. 120, no. 12, pp. 10864–10882, 2015.
[29] M. Blanc and A. D. Richmond, "The ionospheric disturbance dynamo," *J. Geophys. Res., Space Phys.*, vol. 85, no. A4, pp. 1669–1686, 1980.
[30] T. J. Fuller-Rowell, M. V. Codrescu, R. J. Moffett, and S. Quegan, "Response of the thermosphere and ionosphere to geomagnetic storms," *J. Geophys. Res., Space Phys.*, vol. 99, no. A3, pp. 3893–3914, 1994.
[31] D. Buresova, "Effects of geomagnetic storms on the bottomside ionospheric F region," *Adv. Space Res.*, vol. 35, no. 3, pp. 429–439, 2005.
[32] E. Astafyeva, I. Zakharenkova, and M. Förster, "Ionospheric response to the 2015 St. Patrick's Day storm: A global multi-instrumental overview," *J. Geophys. Res., Space Phys.*, vol. 120, no. 10, pp. 9023–9037, 2015.
[33] Y. Wei, B. Zhao, G. Li, and W. Wan, "Electric field penetration into Earth's ionosphere: A brief review for 2000–2013," *Sci. Bull.*, vol. 60, no. 8, pp. 748–761, 2015.
[34] W. Luo, Z. Zhu, C. Xiong, and S. Chang, "The response of equatorial ionization anomaly in 120° E to the geomagnetic storm of 18 August 2003 at different altitudes from multiple satellite observations," *Space Weather*, vol. 15, no. 12, pp. 1588–1601, 2017.
[35] C.-H. Lin, J.-Y. Liu, H.-F. Tsai, and C.-Z. Cheng, "Variations in the equatorial ionization anomaly peaks in the Western Pacific region during the geomagnetic storms of April 6 and July 15, 2000," *Earth Planets Space*, vol. 59, no. 5, pp. 401–405, 2007.
[36] J. Aarons, "Global morphology of ionospheric scintillations," *Proc. IEEE*, vol. 70, no. 4, pp. 360–378, Apr. 1982.
[37] B. Forte, S. M. Radicella, and R. G. Ezquer, "A different approach to the analysis of GPS scintillation data," *Ann. Geophys.*, vol. 45, nos. 3–4, pp. 551–561, 2002.
[38] S. Basu *et al.*, "Two components of ionospheric plasma structuring at midlatitudes observed during the large magnetic storm of October 30, 2003," *Geophys. Res. Lett.*, vol. 321, no. 12, pp. 169–189, 2005.
[39] I. Cherniak and I. Zakharenkova, "Dependence of the high-latitude plasma irregularities on the auroral activity indices: A case study of 17 March 2015 geomagnetic storm," *Earth Planets Space*, vol. 67, no. 1, p. 151, 2015.

YANG LIU received the B.S. and Ph.D. degrees from the School of Electronic Information and Engineering, Beihang University, Beijing, China, in 2006 and 2012, respectively. Since 2012, she has been with the CNS/ATM Laboratory, School of Electronic and Information Engineering, Beihang University. She is currently with the Telecommunications/ICT for Development Laboratory, International Centre for Theoretical Physics, as a one-year Visiting Scientist. She is currently an Assistant Professor with the School of Instrumentation and Opto-Electronic, Beihang University. Her research interests include ionosphere irregularity morphology, ionosphere scintillation, and its effects on GNSS performances.

ZHENG LI received the bachelor's degree from the Beihang University of Optical Engineering, in 2016. He is currently pursuing the master's degree with the School of Instrumentation and Opto-Electronic Engineering, Beihang University, China. His current research interests include ionosphere spatial and temporal studies and ionosphere TEC forecast.

LIANJIE FU received the bachelor's degree from the Shandong University of Science and Technology, in 2016. He is currently pursuing the master's degree with the School of Department of Instrumentation and Opto-Electronic Engineering, Beihang University, China. His current research interests include ionospheric scintillation and precise point positioning.

JINLING WANG received the Ph.D. degree in Geodesy and GNSS from Curtin University, Perth, WA, Australia, in 1999. He is currently an Associate Professor with the School of Civil and Environmental Engineering, University of New South Wales, Sydney, NSW, Australia. His research interests include geospatial mapping and navigation for use in UAS, automated driving as well as indoor environment, with multi-sensor integration, such as integration of GNSS/INS/Vision/LiDAR.

SANDRO M. RADICELLA received the Doctor Honoris Causa degree from the University of Bucharest, Romania, in 2001, and the Doctor of Science degree Honoris Causa from Obafemi Awolowo University, Ile-Ife, Nigeria, in 2005. He is the Head of the Telecommunications/ICT for Development Laboratory (T/ICT4D), Abdus Salam International Centre for Theoretical Physics. He has published about 140 papers in the fields of aeronomy and radio propagation. Among other research topics, he developed models of ionospheric electron density in collaboration with colleagues from ICTP and the University of Graz, Austria. In 2014, he received the Award of Fellowship of the African Geophysical Society.

CHUNXI ZHANG was born in Hengyang, Hunan, China, in 1965. He received the B.S. and M.S. degrees in physics from the China People's Liberation Army Ordnance Engineering College, and the Ph.D. degree in coherent metering technology and instruments from Zhejiang University, China, in 1996. He is currently a Professor with the Department of Instrumentation and Opto-Electronic Engineering, Beihang University, China. His current research interests include advanced optical sensor and sensor network technology, optical inertial navigation technology and integrated navigation, photoelectric measurement and data processing, and optical guidance and navigation. He won the second prize of National Defense Science and Technology of China, in 2000.